Evidence of collisional coherences in the transport of hydrogenic krypton through amorphous carbon foils

Tatsuya Minami,[1] Carlos O. Reinhold,[2] Marek Seliger,[3] Joachim Burgdörfer,[1,3]
Claude Fourment[4], Benoit Gervais[5], Emily Lamour[4], Jean-Pierre Rozet[4] and
Dominique Vernhet[4]

[1] *Department of Physics and Astronomy, University of Tennessee, Knoxville, TN 37996-1200*

[2] *Physics Division, Oak Ridge National Laboratory, Oak Ridge, TN 37831-6373*

[3] *Institute for Theoretical Physics, Vienna University of Technology, A-1040 Vienna, Austria*

[4] *GPS, CNRS UMR 77-88, Universités Paris 7 et 6, 75251 Paris, Cedex 05, France*

[5] *CIRIL, CEA-ISMRA-CNRS UMR 66-37, 14070 Caen, Cedex, France*

(July 27, 2001)

Abstract

We study theoretically and experimentally the population dynamics of the internal state of 60MeV/u Kr^{35+} ions traversing amorphous carbon foils. A quantum transport theory is developed that incorporates the state mixing induced by the wake field of the ion as well as all the coherences generated by the collisional and radiative redistribution of states. We show that the internal state of the ion is sensitive to collisional coherences and the wake field. The results of the full simulations are found to be in good agreement with experimental data.

PACS: 34.50.Fa, 34.10.+x

I. INTRODUCTION

The internal state of a fast ion traversing a solid represents an open quantum system. As the ion traverses the foil, its internal state is altered due to the interaction with the environment, which is made up by particles in the foil and the electromagnetic field. The former leads to multiple collisions which predominantly excites the internal state of the ion to a broad distribution of states. In turn, the latter leads to the radiative decay of the ion, which effectively counteracts the collisional excitation process. In addition to these processes, the ion induces an electric field in the solid (usually referred to as the wake field [1,2]) which produces a Stark-like mixing among the atomic orbitals of the ion. Understanding the interplay among all the processes governing the dynamics of the internal state of the ion has become the objective of numerous works [3–12].

For hydrogen-like atoms or ions, accurate theoretical calculations can be performed and detailed comparisons with experimental data can be made. In this presentation, we focus on the case of 60 MeV/u $Kr^{35+}(1s)$ ions traversing amorphous carbon foils. This system is of particular interest as the radiative lifetime and, hence, the corresponding mean free path is so short that radiative transitions influence the population of excited states inside the solid in direct competition with collisional processes. This requires a treatment of transport in which the collisional and radiative redistribution is treated on the same footing. Our quantum transport theory (QTT) simulating the time evolution of the internal state of the ion is based on a stochastic time dependent Schrödinger equation [13,21]. Multiple collisions for an amorphous foil and radiative decay are stochastic in nature and, after a long propagation time, are expected to yield an incoherent distribution of states. Interestingly, however, we show that the partial coherence of the ionic state directly affects the population dynamics of excited states of the ion and the corresponding line emission intensities. In fact, such effects become clearly visible due to the presence of the wake field of the ion.

The calculations are compared with experimental data obtained at the LISE (Ligne d'Ions Super Epluchés) facility in GANIL (Grand Accélérateur National d'Ions Lourds).

The population dynamics are analyzed by measuring Lyman and Balmer series emitted from the atom by a high resolution spectrometer. To probe the dynamics of the internal state of the ion experimentally, we measure the total intensity of x-rays emitted from the ion as a function of the foil thickness. Atomic units are used throughout unless otherwise stated.

II. THEORY

We consider the transmission of a fast hydrogen-like ion with nuclear charge Z_p and velocity v_p through an amorphous foil. The main objective of our QTT is to describe the time evolution of the populations, P_i, of the excited states of the ion. We use time, t, or propagation path in the laboratory frame, d, indistinguishably since $d = v_p t$ and $v_p = \text{Const.}$. The zero $t = 0$ corresponds to the time at which the ion enters the foil. For simplicity, we will use a single index $|i\rangle$ to label the eigenstates of the ion in vacuum, with the implicit understanding that $|i\rangle = |n\ell\jmath m_\jmath\rangle$, where n is the principal quantum number, ℓ is the orbital angular momentum, and $\jmath$ and $m_\jmath$ are the total angular momentum and its projection onto the z-axis. The quantization axis corresponds to the direction of propagation (i.e. z-axis $\parallel \vec{v}_p$).

Our total system consists of the hydrogen-like ion, the amorphous carbon foil and the electromagnetic field. If we denote the state of the total system at a certain time t by a density matrix $\rho(t)$, its time evolution is governed by the Liouville equation,

$$i\frac{\partial}{\partial t}\rho(t) = [\mathcal{H}_{tot}, \rho(t)], \tag{2.1}$$

where $\mathcal{H}_{tot}$ is the Hamiltonian of the total system and [,] is a commutator. The reduced density matrix $\sigma(t)$ containing all the information about the internal state of the ion can be obtained by tracing $\rho(t)$ with respect to the degrees of freedom of the environment: i.e. $\sigma(t) \equiv \text{Tr}'[\rho(t)]$. For example, the population or occupation probability to be in state $|i\rangle$ is given by $P_i(t) = \sigma_{i,i}(t) = \langle i|\sigma(t)|i\rangle$. The time evolution of $\sigma(t)$ is governed by a Liouville equation with a dissipative term

$$i\frac{\partial}{\partial t}\sigma(t) = [\mathcal{H}_{atom}, \sigma(t)] + \mathcal{R}\sigma(t), \tag{2.2}$$

where $\mathcal{R}$ is a relaxation superoperator that represents the interaction between the electron and the environment. In the above equation, $\mathcal{H}_{atom}$ is a time-independent Hermitian Hamiltonian describing the non-dissipative evolution of the electron in the ion,

$$\mathcal{H}_{atom} \equiv \frac{p^2}{2} - \frac{Z_p}{r} + V_{scr}(\vec{r}) \quad + \quad \Delta\mathcal{H}_{rel} \quad , \tag{2.3}$$

where r and p are the position coordinate and the momentum of the electron in a reference frame fixed to the ion, and $\Delta\mathcal{H}_{rel}$ represents relativistic and Lamb corrections. In Eq. (2.3) $V_{scr}(\vec{r})$ denotes the screening potential or wake potential induced by the ion. For convenience, we define $\mathcal{H}_0$ as the internal Hamiltonian of the ion in vacuum,

$$\mathcal{H}_0 \equiv \frac{p^2}{2} - \Delta\mathcal{H}_{rel} \quad + \quad \frac{Z_p}{r} \quad , \tag{2.4}$$

whose eigenvalues and eigenenergies are given by

$$\mathcal{H}_0|i\rangle = E_i|i\rangle \ . \tag{2.5}$$

The explicit construction of $\mathcal{R}$ in Eq. (2.2) is, in general, a formidable task since it involves the many-body dynamics of the environment to which the open system couples. The simplifying assumption which makes the determination of $\mathcal{R}$ feasible is perturbation theory, according to which the dynamics of the environment remains decoupled from σ. Even after the evaluation of $\mathcal{R}$ within perturbation theory, solving the Liouville equation is a tedious task. The Liouville equation could be solved using an expansion of the density matrix in a finite basis set of eigenstates $|i\rangle$, $i = 1, 2, ..., N$, where N is the rank of the expansion. This reduces the Liouville equation to a finite system of N^2 coupled equations. Since the representation of the density matrix has rank N^2, a finite representation of $\mathcal{R}$ involves N^4 elements. This makes the explicit solution of the Liouville equation difficult.

The simplest approximation to the Liouville equation consists of neglecting the couplings between the off-diagonal matrix elements of the density matrix ($\sigma_{i,j}$, $i \neq j$) and the diagonal matrix elements. This reduces the system of N^2 coupled equations to a system of N equations usually referred to as rate equations:

$$\frac{d}{dt}\sigma_{i,i}(t) = \sum_{i,j} \Gamma_{i\to j}\sigma_{i,i}(t) - \Gamma_j \sigma_{j,j}(t) \tag{2.6}$$

where $\Gamma_j = \sum_i \Gamma_{i\to j}$ is the inverse of the lifetime of state $|i\rangle$ and $\Gamma_{i\to j}$ is the transition rate per unit time from state $|i\rangle$ to state $|j\rangle$ induced by the environment, which can be decomposed into collisional, radiative and wake mixing rates, $\Gamma_{i\to j} = \Gamma^{coll}_{i\to j} + \Gamma^{rad}_{i\to j} + \Gamma^{wake}_{i\to j}$.

The system of rate equations (2.6) usually provides a reasonable overall description of the time evolution of the populations. However, clear evidence of its limitations are abundant and are due to the disregard of coherences (i.e. off-diagonal matrix elements of the density matrix). Recently, the explicit treatment of coherences has been incorporated within quantum transport approaches [13,15,16]. One of these approaches directly solves the Liouville equation as a system of coupled equations. In order to accomplish this, in Refs. [15,16] estimates were made to select a small number of active off-diagonal elements of σ such that the dominant elements of $\mathcal{R}$ could be stored in the memory of computers. In this paper, we adopt an alternative scheme which keeps all elements of σ and all couplings to the environment but avoids dealing directly with a finite representation of $\mathcal{R}$. This can be accomplished using a Monte Carlo method along the lines of Refs. [13,14]. This method is, in the limit of vanishing sampling error, equivalent to solving Eq. (2.2) but involves only matrices with dimension N^2. We refer to this method as quantum transport theory (QTT).

The main idea behind the QTT is that the reduced density matrix $\sigma(t)$ can be decomposed as an incoherent average over pure states [17]. If the electron is initially, at $t = 0$, in a pure state $|0\rangle$,

$$\sigma(t) = \frac{1}{N_{traj}} \sum_{\mu=1}^{N_{traj}} |\psi^\mu(t)\rangle\langle\psi^\mu(t)| \,, \tag{2.7}$$

where N_{traj} denotes the number of pure states (or quantum trajectories) involved in the average whose boundary condition is

$$|\psi^\mu(t=0)\rangle = |0\rangle \quad . \tag{2.8}$$

Thus, solving Eq. (2.2) within the QTT reduces to calculating the wavefunctions $\psi^\mu(t)$ followed by the averaging in Eq. (2.7). In numerical simulations, the total number of quan-

tum trajectories, N_{traj}, has to be large enough so that the right hand side of Eq. (2.7) converges. Each of the wavefunctions is called a quantum trajectory and describes a different random sequence of interactions with the environment. The stochastic time evolution of the quantum trajectories is calculated by constructing their corresponding time evolution operator $U^{\mu}(t,0)$ such that

$$|\psi^{\mu}(t)\rangle = U^{\mu}(t,0)|0\rangle \quad . \tag{2.9}$$

We decompose the time evolution operator into a product of two types of evolution operators:

$$U^{\mu}(t,0) = U^{\mu}_{cont}(t,t_n) \prod_{k=1}^{n} U^{\mu}_{dis}(t_k) U^{\mu}_{cont}(t_k,t_{k-1}) \quad , (t_0 = 0). \tag{2.10}$$

One type, $U^{\mu}_{cont}(t_{k+1},t_k)$, stands for a continuous change of the wavefunction during the time period $[t_{k+1},t_k]$. The other type, $U^{\mu}_{dis}(t_k)$, induces a discontinuous change of the wavefunction (a quantum jump) at randomly chosen times $t = t_k$. Finite representations of these operators have dimension N^2 and are easier to treat numerically than the full representation of $\mathcal{R}$ in Eq. (2.2). Recently, procedures have been developed for constructing random subsets of quantum jump times $\{t_k\}$ and the quantum jump operators which yield the correct relaxation superoperators for both radiative decay [18,19] and multiple collisions [13,21].

The present QTT easily allows us to investigate the relative role of coherences in the population dynamics. For example, one can eliminate coherences by multiplying the matrix elements of the evolution operator by random phases: i.e. replacing $\langle i|U^{\mu}_{cont}|j\rangle$ by $\langle i|U^{\mu}_{cont}|j\rangle \times \exp(i\phi_{i,j})$, where $\phi_{i,j}$ are independent random phases uniformly distributed in the interval $(0,2\pi)$. In this case, the time evolution becomes equivalent to the system of incoherent rate equations (2.6). We investigate in this paper the role of collisional coherences by multiplying random phases the matrix elements of collisional jumps $U^{\mu}_{dis}(t_k)$.

III. EXPERIMENT

Our experiment has been performed at GANIL on the LISE facility. The complete experimental set-up has been already described in detail elsewhere [20]. Here we summarize

its main characteristics. Beams are directed onto self-supported amorphous carbon foils with measured thicknesses and purity [20]. The foils can be tilted to change the effective transport thickness. Foil thicknesses are changed from 3 to 220 μg/cm^2 to study the ion transport from near single collision to equilibrium limit. Balmer α lines are also measured using high-resolution high-transmission Bragg-crystal spectrometers. Each photon detection system is placed at a specific angle with respect to the beam direction to assure polarization-insensitivity of the measurements.

From the Balmer lines (see Table 1) and branching ratios (see Table 1), we can obtain the ratio between the total intensities of photons emitted from the $3p_{1/2}$ and $3s_{1/2}$ states as well as from the $3d_{3/2}$ and $3d_{5/2}$ states,

$$\frac{I_{3p_{1/2}}}{I_{3s_{1/2}}} = \frac{1}{0.1874}\left(\frac{Ba_4}{Ba_1} - 0.5507\right) \tag{3.1}$$

and

$$\frac{I_{3d_{3/2}}}{I_{3d_{5/2}}} = 6.502\frac{Ba_2}{Ba_3}. \tag{3.2}$$

Details of this analysis are explained in Ref. [20]. Differences between the coefficients above and those in Ref. [20] are due to the relativistic corrections to the radiative transition rates.

The total photon intensity of all lines emitted from a particular level is given by

$$I_i = \Gamma_i^{rad}\int_0^\infty dt P_i(t). \tag{3.3}$$

This intensity provides direct information on the time integral of the population $P_i(t)$ (weighted by a constant transition rate). Note that the time integral involves the population while the ion is both inside the solid and after foil exit. Therefore, the population is initially zero, increases due to excitation inside the foil, and tends to zero again for $t \to \infty$, when the atom relaxes to the ground state by radiative decay after foil transmission. Since transport through foils of different thickness yield different intermediate populations, changes in the line intensities provide direct evidence of the changing behavior of the populations due to transport. Since energy levels are independent of m_j, the experimentally observable intensities correspond to

$$I_{n,\ell,\jmath} = \sum_{m_\jmath} I_{n,\ell,\jmath,m_\jmath} \tag{3.4}$$

which provide direct information on the populations of the $n, \ell, \jmath$-subshells.

IV. RESULTS

Figure 1 displays results of realistic transport simulations of 60MeV/u $Kr^{35+}(1s)$ ions traversing amorphous carbon foils. The figure shows the populations of the $3p_{1/2}$ and $3s_{1/2}$ energy levels at the foil exit as a function of the foil thickness. The populations first increase monotonically and subsequently reach a plateau. The increase of the populations is due to multiple collisions which excite the electron from the 1s state into these levels. For increasing foil thickness a plateau is reached as the 1s state of Kr starts to become considerably depleted and while, simultaneously, the excited states are also depleted by multiple collisions. For foils thicknesses beyond those depicted in the figure, the populations decrease monotonically as a function of foil thicknesses and ionization starts playing an important role. Here we discuss ion-solid interactions for foil thicknesses less than 2.5×10^4 a.u., which is the maximum foil thickness utilized in our experiment. In this region, energy levels are mostly populated by direct transitions from the ground state rather than from multiple excitations involving several n-levels. In turn, there exists a large degree of intrashell collisional and wake-induced mixing. The calculations were obtained using an expansion of the wavefunction of the projectile electron in a basis set involving bound states of the ion in the energy levels $1 < n < 6$, which corresponds to a total number of 182 states. The ionization probability in typical experiments is small and, therefore, using this basis is a good approximation. For $V_{sc}(\vec{r})$, we use the n dependent electric field from Ref. [15].

In order to analyze the effect of collisional coherences, we display in Fig. 1 simulations with and without collisional coherences. Clearly, ignoring collisional coherences leads to departures from the full transport simulations. These departure become pronounced in Figure 2, which displays the ratio of the populations as a function of foil thickness as well as the relative emission intensities. For very thin foils, these ratios are equal to the ratio

between the excitation probability from the 1s state to the $3p_{1/2}$ and $3s_{1/2}$ states under single collision conditions. For increasing foil thicknesses, the ratios provide information on the time development of the internal state of the ion. In the absence of either the wake field or collisional coherences, the populations of the $3p_{1/2}$ and $3s_{1/2}$ states become very similar for thick foils. However, collisional coherences in combination with the wake field shifts the population systematically towards the $3p_{1/2}$ state. This is due to the fact that for the relative phases associated with the excitation process, the wake field tends to increase the ratio of the $3p_{1/2}$ population to the $3s_{1/2}$ population. Clearly, since the two levels are coupled by the wake field, the initial coherence between the two levels plays a crucial role in the time evolution of the population ratio for thin foils. Only inclusion of both the wake field and collisional coherences leads to the proper intrashell mixing of states and yields photon intensities that are in good agreement with the experimental data. It is also noteworthy that the calculated ratio $I_{3p_{1/2}}/I_{3s_{1/2}}$ obtained from the full QTT simulation increases for increasing foil thickness whereas the ratio of the populations at the foil exit are a decreasing function of foil thickness. This is a direct consequence of radiative decay during transport.

In summary, in order explain the experimental findings, we find that the Stark mixing and collisionally induced coherences between the $3s_{1/2}$ and $3p_{1/2}$ states needs to be accounted for within the transport simulations. The experiment provides clear evidence of the interplay between the wake field and collisional coherences.

ACKNOWLEDGMENTS

This work was supported by the NSF and FWF (Austria). COR acknowledges support by the DCS, OBES, USDOE, managed by UT-Battelle, LLC, under contract DE-AC05-00OR22725.

REFERENCES

[1] P. Echenique, W. Brandt and R. H. Ritchie, Phys. Rev. B, **33**, 43(1979)

[2] P. M. Echenique, F. Flores, and R. H. Ritchie, Solid State Phys. **43**, 229 (1990).

[3] J. Kemmler, J. Burgdörfer, and C.O. Reinhold, Phys. Rev. A **44**, 2993 (1991).

[4] C. O. Reinhold, D. G. Arbó, J. Burgdörfer, B. Gervais, E. Lamour, D. Vernhet and J-P. Rozet, J. Phys. B, **33**, L111(2000)

[5] J. Burgdörfer and J. Gibbons, Phys. Rev. A, **42**, 1206(1990)

[6] Y. Yamazaki et al., Phys. Rev. Lett. **61**, 2913 (1988).

[7] P. Nicolai, M. Chabot, J.P. Rozet, M.F. Politis, A. Chetioui, C. Stéphan, A. Touati, D. Vernhet, and K. Wohrer, J. Phys. B **23**, 3609 (1990).

[8] J. Burgdörfer and C. Bottcher, Phys. Rev. Lett. **61**, 2917 (1988).

[9] J.P. Rozet, C. Stéphan, and D. Vernhet, Nuc. Inst. Meth. B **107**, 67 (1996).

[10] H.D. Betz, D. Röschenthaler, and J. Rothermel, Phys. Rev. Lett. **50**, 34 (1983). J. Rothermel, H.D. Betz, and F. Bell, Nuc. Inst. Meth. **194**, 341 (1982).

[11] C. Can, R.J. Maurer, B. Bandong, and R.L. Watson, Phys. Rev. A **35**, 3244 (1987).

[12] D. Vernhet, J.P. Rozet, E. Lamour, B. Gervais, C. Fourment, and L.J. Dubé, Phys. Script. **T80A**, 83 (1999).

[13] D. G. Arbó, C. O. Reinhold, P. Kürpick, S. Yoshida and J. Burgdörfer, Phys. Rev. A, **60** 1091(1999)

[14] D. G. Arbó, C. O. Reinhold, S. Yoshida and J. Burgdörfer, Nucl. Inst. Methods Phys. Res. B, **164-165**, 495(2000)

[15] J-P Rozet, D. Vernhet, I. Bailly-Despiney, C. Fourment and L. J. Dubé, J. Phys. B, **32**, 4677(1999)

[16] D. Vernhet, C. Fourment, E. Lamour, J-P. Rozet, B. Gervais, L. J. Dubé, F. Martin, T. Minami, C. O. Reinhold, M. Seliger and J. Burgdörfer, Physica Scripta, **T91**, in press(2001)

[17] U. Fano, Rev. Mod. Phys. **29**, 74(1957)

[18] J. Dalibard, Y Castin, and K. Mølmer, Phys. Rev. Lett., **68**, 580(1992); K. Mølmer, Y Castin, and J. Dalibard, J. Opt. Soc. Am. B, **10**, 524(1993)

[19] R. Dum, P. Zoller and H. Ritsch, Phys. Rev. A, **45**, 4879(1992); C. W. Gardiner and P. Zoller, *Quantum Noise* (Springer, 1999)

[20] D. Vernhet, J-P. Rozet, I. Bailly-Despiney, C. Stéphan, A. Cassimi, J-P. Grandin and L. J. Dubé, J. Phys. B, **31**, 117(1998)

[21] T. Minami, C.O. Reinhold, M. Seliger, J. Burgdörfer, C. Fourment, B. Gervais, E. Lamour, J.P. Rozet, and D. Vernhet, in preparation.

Table 1: Labeling and branching ratios of the Balmer lines.

Transition	Label	Branching ratio
$3s_{1/2} \rightarrow 2p_{3/2}$	Ba_1	0.64485
$3d_{3/2} \rightarrow 2p_{3/2}$	Ba_2	0.15379
$3d_{5/2} \rightarrow 2p_{3/2}$	Ba_3	1.
$3p_{1/2} \rightarrow 2s_{1/2}$	Ba_{4a}	0.12087
$3s_{1/2} \rightarrow 2p_{1/2}$	Ba_{4b}	0.35515
$3p_{3/2} \rightarrow 2s_{1/2}$	Ba_{5a}	0.12340
$3d_{3/2} \rightarrow 2p_{1/2}$	Ba_{5b}	0.84621

FIGURES

FIG. 1. Populations of the $3p_{1/2}$ and $3s_{1/2}$ states at foil exit as a function of foil thickness. Solid lines: full calculation. Dotted lines: calculation without collisional coherences.

FIG. 2. Population ratio and line emission intensity ratio as a function of foil thickness. Symbols with error bars: experiment. Solid lines: full calculation. Dashed lines: calculation without the wake field but with collisional coherences. Dotted lines: calculation without collisional coherences but with wake field.

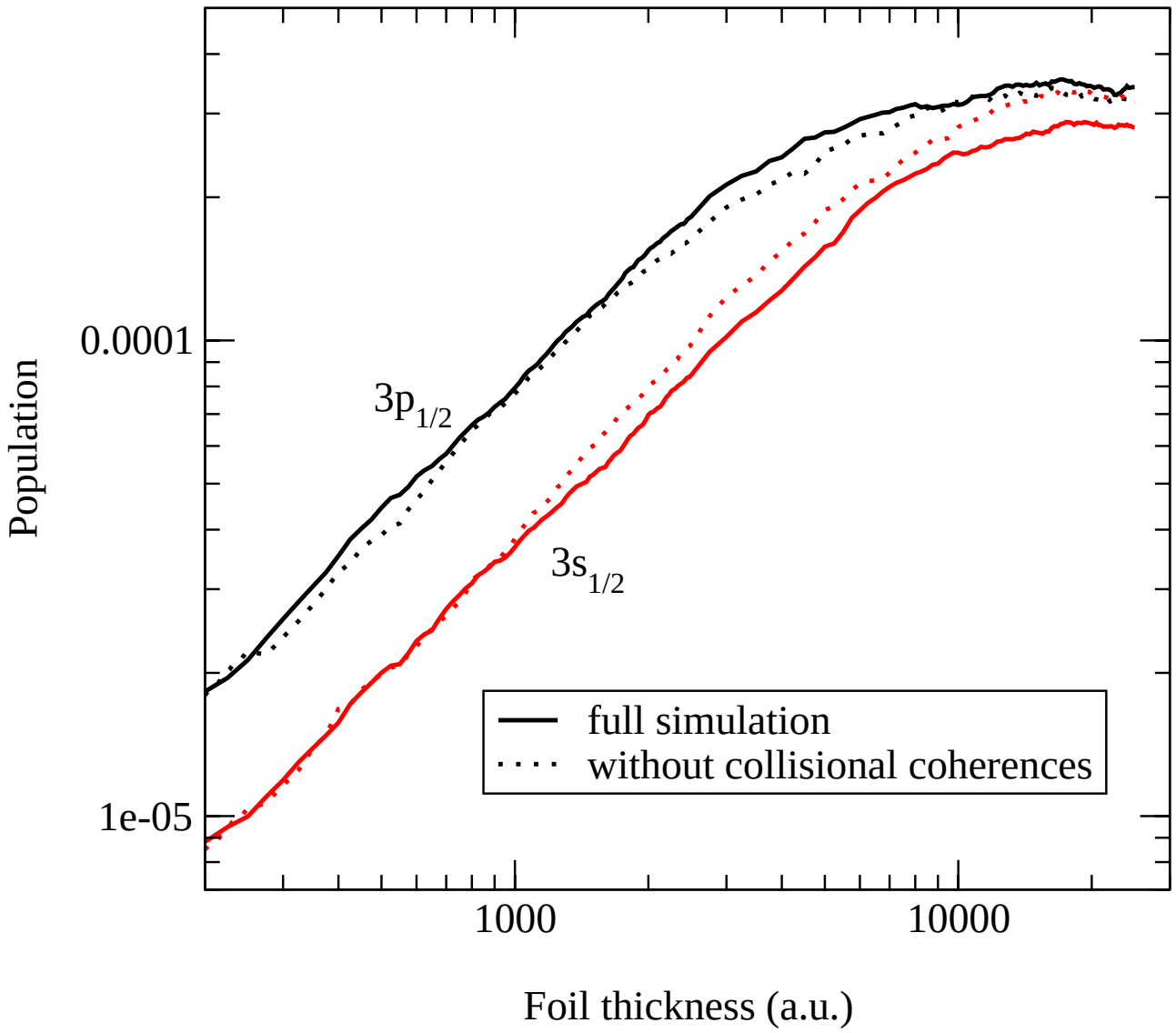
Population
0.0001
1e-05
1000
10000
Foil thickness (a.u.)
3p1/2
3s1/2
full simulation
without collisional coherences

Fig. 1

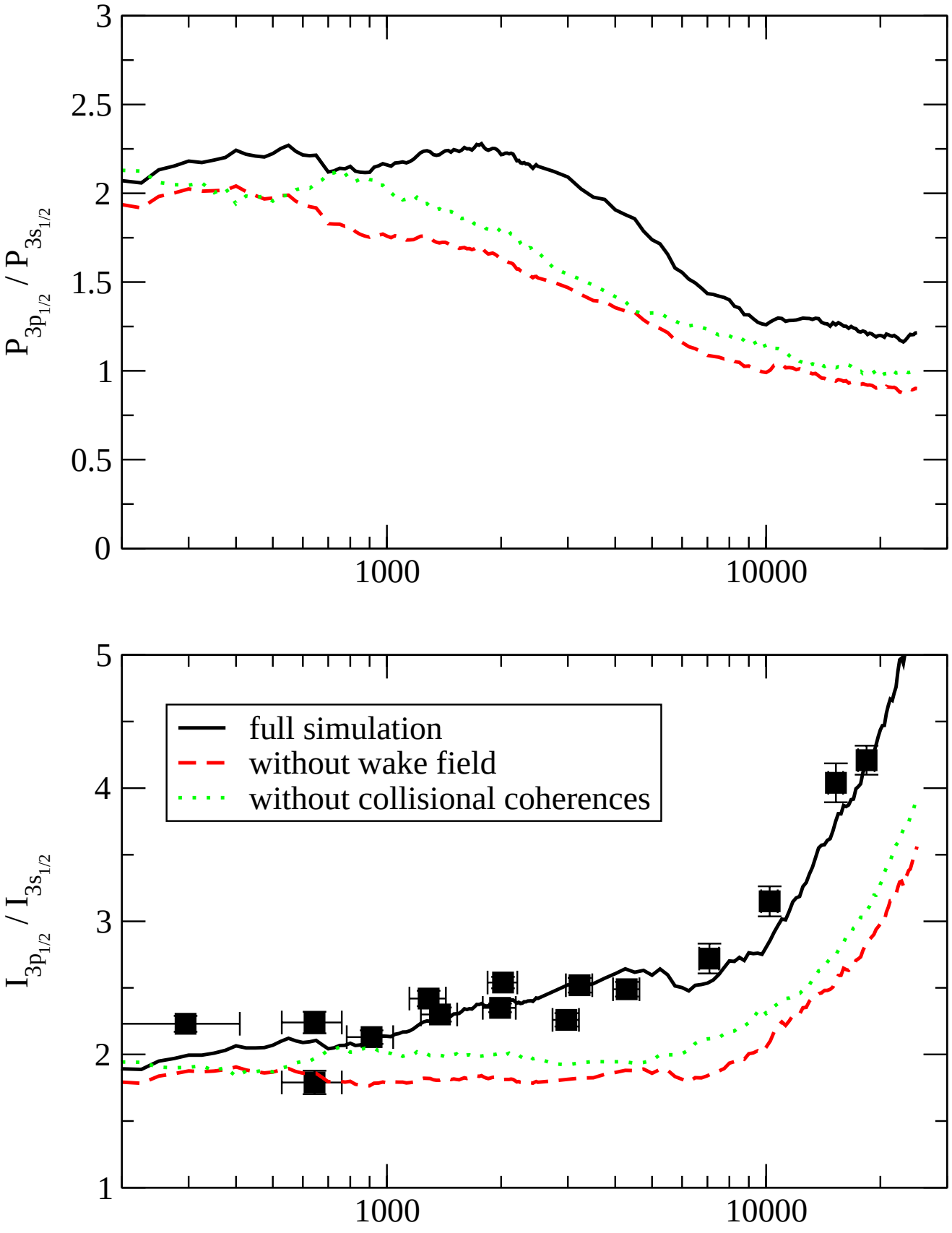
3
2.5
2
1.5
1
0.5
0
1000
10000
$P_{3p_{1/2}} / P_{3s_{1/2}}$
5
4
3
2
1
1000
10000
$I_{3p_{1/2}} / I_{3s_{1/2}}$
full simulation
without wake field
without collisional coherences
Foil thickness (a.u.)

Fig.2